mission planning. These missions show that there will be no biological hazard associated with passage through the trapped radiation belts during the translunar and trans-Earth phase of Apollo lunar missions, providing that there are no further high-altitude nuclear tests and that astronaut activity is confined to the command module during belt passage.

The Apollo 4 and 6 radiation analysis shows that a certain degree of proficiency has been obtained in estimating the potential radiation encountered by spacecraft passing through the trapped radiation belts. However, since the possibility of a radical change in the trapped radiation environment exists, manned space vehicles will be supplied with sufficient radiation-monitoring instrumentation to provide real-time evaluation of this environment.

References

[1] Higgins, P. W., Lill, J. C., and White, T. T., *Radiation Environment at High Orbital Altitudes*, NASA SP-138, 1967, pp. 149–157.

[2] Richmond, R. G. et al., *Radiation Dosimetry for Manned Space Flight*, NASA SP-169, 1968, pp. 555–580.

[3] McIlwain, C. E., "Coordinates for Mapping the Distribution of Magnetically Trapped Particles," *Journal of Geophysical Research*, Vol. 66, Nov. 1961, pp. 3681–3691.

[4] Jensen, D. C. and Cain, J. C., "An Interim Geomagnetic Field," *Journal of Geophysical Research*, Vol. 67, Aug. 1962, pp. 3568–3569.

[5] Vette, J. I., *Models of the Trapped Radiation Environment Vol. I: Inner Zone Protons and Electrons*, NASA SP-3024, 1966.

[6] Vette, J. I., Lucero, A. B., and Wright, J. A., *Models of the Trapped Radiation Environment, Vol. II: Inner and Outer Zone Electrons*, NASA SP-3024, 1966.

[7] Bostrom, C. O. and Williams, D. J., "Time Decay of the Artificial Radiation Belt," *Journal of Geophysical Research*, Vol. 70, Jan. 1965, pp. 240–242.

[8] Hardy, A. C., Lopez, M. D., and White, T. T., *A Parametric Technique of Computing Primary Electron Dose*, edited by A. Reetz and K. O'Brien, NASA SP-169, 1968, pp. 391–401.

[9] Chapman, M. C. et al., "Phase I Analysis of Data Returned by the FESS Experiment from the OV 1-2 Spacecraft," Contract AF 29(601)-7038, AFWL-TR-66-94, March 1967, U.S. Air Force.

[10] Thede, A. L. and Radke, G. E., *A Correlation of Dosimetric Measurements with Charged Particle Environment of the Inner Van Allen Belt*, edited by A. Reetz and K. O'Brien, NASA SP-169, 1968, pp. 75–92.

JULY 1970 J. SPACECRAFT VOL. 7, NO. 7

Model for the Prediction of Closed Compartment Fire Propagation

M. Bello* and A. L. Johnson†
The Aerospace Corporation, El Segundo, Calif.

A one-dimensional (radial) mathematical model of a closed compartment fire is developed to 1) analyze the effects of various combustion parameters and 2) predict the composition, pressure, and temperature histories of the atmosphere during a fire. A semiempirical expression is formulated to relate the average linear burning rate of the combustile materials and the flame propagation which includes the effects of convective velocity, gravity, total pressure. and oxygen partial pressure. A computer program is used to solve the equations resulting from the heat, mass, and combustion equations. The results of this analysis provide a macroscopic overview of a fire in a closed compartment.

Nomenclature

A = surface area of compartment, in.^{2}
a = surface area of a sphere ($4\pi r^2$), in.^{2}
C_g = thermal capacitance of gaseous atmosphere, Btu/°R
C_m = thermal capacitance of compartment mass, Btu/°R
c_p = specific heat at constant pressure, Btu/lb-°R
g = magnitude of gravitational field, ft/sec^2
Gr = Grashof number
h = film coefficient, Btu/in.^{2}-sec-°R
Δh_c = heat of combustion of burning material, Btu/lb
k = thermal conductivity of gas, Btu/in.-°R-sec
L = characteristic length, in.
l = linear sample burn distance, in.
Nu = Nusselt number
Pr = Prandtl number
P_T = total atmospheric pressure, psia
$\dot{q}_k$ = gas conduction heat rate, Btu/sec
$\dot{q}_c$ = convective heat rate, Btu/sec
$\dot{q}_v$ = heat of evaporization or condensation, Btu/sec
$\dot{q}_r$ = radiation heat rate, Btu/sec
$\dot{q}_T$ = total heat rate from the combustion region, Btu/sec
$\dot{q}_\beta$ = burning rate heat rate, Btu/sec; $\dot{q}_{\beta 1}$, to gas; $\dot{q}_{\beta 2}$, to mass
R_k = conduction resistance, sec-°R/Btu
R_c = convection resistance, sec-°R/Btu
R_r = radiation resistance, sec-°R/Btu
r = radius of spherical flame front, in.
r_i = radius of initial flame front, in.
r_o = radius of spherical model, in.
r_s = equivalent radius of sample, in.
Re = Reynolds number
T_f = flame temperature, °F
T_g = bulk gas temperature, °F
T_m = bulk equipment mass temperature, °F
t = time (independent variable), sec
V = volume of material, in.^{3}
v = velocity of circulating gas, in./sec
W = mass, lb
x = experimental exponents
Y = mole fraction
y = experimental exponents
α = area burning rate, in.^{2}/sec
β = convective linear burning rate, in./sec
β_s = experimental linear burning rate of a particular sample, in./sec

Presented as Paper 69-618 at the AIAA 4th Thermophysics Conference, San Francisco, Calif., June 16–18, 1969; submitted December 4, 1969, revision received February 24, 1970.

* Member of the Technical Staff, Thermal Systems and Cryogenics Section, Applied Mechanics Division.

† Section Manager, Thermal Systems and Cryogenics Section, Applied Mechanics Division.

β^* = total linear burning rate, in./sec
γ = volume burning rate, in.^{3}/sec
ϵ = total emissivity due to flame luminosity, dimensionless
θ,θ' = topological functions for convection (geometry, gravity) and for conduction and radiation (geometry), respectively
ξ = ratio of volumetric heats of combustion, ϕ'/ϕ
$\bar{\rho}$ = average density of burning material, lb/in.^{3}
σ = Stefan-Boltzmann constant, Btu/in.^{2}-°R^4-sec
τ = linearized radiation constant, °R^3
ϕ = volumetric heat of combustion, Btu/in.^{3}
ψ = McAlevy correlation factor

Introduction

IN the past few years, considerable effort has been expended by the aerospace industry to minimize the fire hazard in oxygen-enriched environments.‡ However, despite stringent material specification and careful equipment design, the complete inhibition of a fire in an oxygen-enriched compartment is not practical. Therefore, an analytical model of a fire in a fixed-volume, fixed-mass compartment has been developed in an effort to provide guidance with respect to the effects of various combustion parameters and the composition, pressure, and temperature histories of the compartment atmosphere during a fire. The one-dimensional (radius for a spherical system) analytical solution is derived utilizing heat and mass balances and material combustion characteristics. A computer program is used to solve the resulting equations.

In a closed compartment, the combustion of organic materials (specifically, hydrocarbon fuels out-gassed from organic materials) appears to be more probable than the combustion of inorganic materials. Further, nonhydrocarbons or materials containing O, N, Si, etc., have much lower heats of combustion than organic materials, so that basing the analysis on hydrocarbons will lead to conservative results. Hydrocarbons of reasonable molecular weight can be approximated by $(CH_2)_n$ such that complete combustion would give CO_2 and H_2O. However, combustion studies have shown that free carbon is formed when typical hydrocarbon materials are burned[1,2] such that

$$2(CH_2)_n + 2nO_2 \rightarrow nC + nCO_2 + 2nH_2O \quad (1)$$

For incomplete combustion

$$2(CH_2)_n + \tfrac{5}{2}nO_2 \rightarrow nCO + nCO_2 + 2nH_2O \quad (2)$$

Equation (2) is of interest because CO is toxic, and it closely represents a smoldering type fire. However, it is known that the reaction producing CO_2 generates $2\frac{1}{2}$ times more heat than the reaction producing CO.[3] In order to maintain a worst-case model from the standpoint of energy release, Eq. (2) will be used in this analysis to represent the combustion of solid materials in a spacecraft fire.

Analysis

The model (Fig. 1a) assumes that a spherical fire begins in the center of the compartment and that the flame front propagates outward (radially). This one-dimensional assumption simplifies the equations; further, in the absence of gravity, it has been shown[4] that the flame front burns in a symmetrical form. The arrows show the advancing spherical flame front, the shaded area represents the burnt material, and the outer shell represents the thermal mass of all the solid materials present. The lumped-parameter representation of this model is shown in Fig. 1b.

The assumption of a sealed, fixed-volume, fixed-mass compartment is made to simplify the model. (No gas enters or leaves.) Hence, the pressures predicted from this analysis, which are for a fire in a sealed compartment, are higher than would be realized during a fire in an actual, imperfectly sealed compartment. The oxygen concentration also may be somewhat higher. Therefore, the model is somewhat conservative. This model will not handle the case in which an oxygen line is severed within the compartment, since the assumption of a fixed mass system would be violated.

A constant flame temperature of 3600°R is assumed. Since hydrocarbon flame temperatures could vary from 3200–3600°R depending on the fuel and its surroundings, this assumption also tends to make the analysis conservative.

In the lumped-parameter analog of Fig. 1b, three nodes are utilized: 1) a forcing temperature node (flame temperature), 2) a gas node, and 3) a bulk-mass node. If a fixed flame temperature is assumed, the thermal capacitance (the product of the mass and specific heat of the node) of the flame is infinite. The thermal capacitances of the gas and the bulk-mass are represented in this model by the assumption that all the gas in the compartment can be lumped into one gas node, and all solid material assumed to be uniformly distributed in the compartment can be lumped into one bulk-mass node. The assumption that all the energy is conserved within the compartment makes the model adiabatic; this is a conservative assumption, because in the actual case the compartment or cabin would transfer energy into the surroundings.

It is further assumed that the compartment atmosphere is always homogeneous; i.e., the oxygen in the container is always available at the flame front at its existing partial pressure during the combustion process. This assumption is conservative, because it removes the classical diffusion barrier between the oxygen supply and the flame front which usually controls flame propagation in a static gas environment and in zero-g. The effect of the condensation of the water produced in the combustion reaction was considered and was found to be negligible.

Derivation of Basic Equations

From the lumped-parameter network shown in Fig. 1b, the following heat fluxes are defined:

$$\dot{q}_k = (T_f - T_g)/R_k, \quad R_k = (r_o - r)/4\pi k r_o r \quad (3)$$

where

$$\dot{q}_r = (T_f - T_m)/R_r, \quad R_r = 1/\sigma\epsilon\tau a \quad (4)$$

where

$$\tau = [T_f^3 + T_f^2 T_m + T_f T_m^2 + T_m^3] \approx 5.59 \times 10^{10}$$

for $T_f = 3600°R$; $T_m = 500°$R

$$\dot{q}_c = (T_g - T_m)/R_c, \quad R_c = 1/hA \quad (5)$$

The gas conduction term between the flame and the bulk gas mass can be expressed in terms of two concentric spheres: the

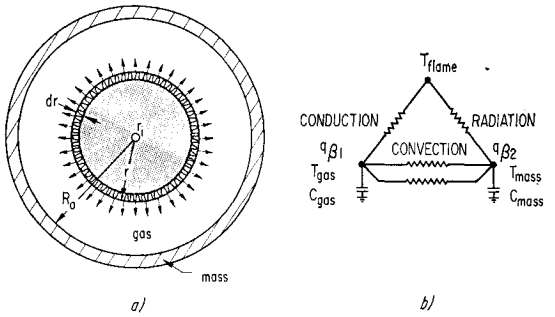

Fig. 1 Fire model. Assumptions: 1) fixed volume, no atmosphere enters or leaves container; 2) mass distribution expressed as lumped nodes; 3) energy relation expressed in terms of lumped parameters; 4) constant frame temperature; 5) spherical flame front always centered within spherical container; 6) gas radiation on terms negligible.

‡ Environments having an oxygen concentration higher than that in air.

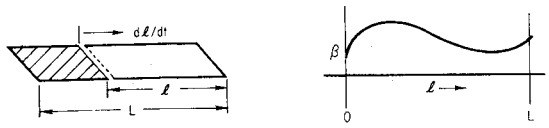

Fig. 2 Representation of linear burning rate.

outer sphere is fixed and used to represent the bulk mass, while the inner sphere represents the moving flame front. It should be noted that Eq. (3) breaks down as $r \to R$; however, in the cases examined the combustion process terminated due to oxygen depletion before r reached 50% of r_o.

Heat balances at both the gas and bulk-mass nodes produce the following differential equations:

$$C_g(dT_g/dt) = \dot{q}_k - \dot{q}_c - \dot{q}_v + \dot{q}_{\beta 1} \quad (6)\S$$

$$C_m(dT_m/dt) = \dot{q}_r + \dot{q}_c + \dot{q}_v + q_{\beta 2} \quad (7)$$

where

$$C_g = W_g\bar{c}_p = (Wc_p)_{O_2} + (Wc_p)_{CO_2} + (Wc_p)_{H_2O} + (Wc_p)_{\text{diluent}}$$

$$\dot{q}_{\beta 1} = hA_f(T_f - T_g) - h(4\pi r^2)(T_f - T_g)$$

$$\dot{q}_{\beta 2} = hA_{\text{cont}}(T_f - T_m) = h(4\pi r_o^2)(T_f - T_m)$$

In the estimation of C_g, both the unreacted gaseous constituents and the gaseous products of combustion are considered. (The relationship of $\dot{q}_{\beta 1}$ and $\dot{q}_{\beta 2}$ to the burning rate heat flux $\dot{q}_\beta$ is shown later.)

If the energy of ignition is disregarded, it is possible to relate the total energy leaving the flame front to the amount of material being consumed in the combustion process. Note that the assumed constant flame temperature implies that the energy exchange between the flame front and the vaporizing fuel can be neglected without altering the over-all material and energy balance.

$$\dot{q}_T = \bar{\rho}\Delta h_c(dV/dt) = \phi(dV/dt) \quad (8)$$

In order to estimate the rate of flame spread during a fire in a compartment, it is first necessary to define material linear burning rate. The linear burning rate of a sample is represented in Fig. 2 and is defined as either the average rate or the rate at a particular $l \simeq L/2$. For the standard burning test setup used to determine this rate, the effects of radiation and conduction are minimized and the atmosphere is of sufficient capacity that the bulk composition does not change significantly. The linear burning rate β^* is defined as $\beta^* = (dl/dt)_{1-g}$. Heuristic reasoning leads to the definition of an area burning rate, $\alpha \equiv dA/dt$, and a volume burning rate, $\gamma \equiv dV/dt$. Further, if one assumes that $\alpha = \alpha(\beta^*)$, and $\gamma = \gamma'(\alpha)$, it is possible to define a relationship $\gamma = \gamma(\beta^*)$.

Physically, β^* is determined by burning a strip of material in a special atmosphere in a 1-g field using a specifically defined test setup. In the absence of gravity, experimental evidence shows that the strip will still burn, and the physics indicate that the rate is based on the equilibrium between radiation-conduction heat balance and gaseous diffusion of O_2 to the flame area. With the presence of gravity, the combustion is much faster. It is possible, therefore, to infer that

$$\beta^* = \beta^*[(lg)^n, \theta_f(P_{T_1}P_{O_2}), \quad (\dot{q}_r + \dot{q}_k)/\phi] \quad (9)$$

Hence, it is possible to deduce that γ^* is a function of the same parameters.

Material linear burning rates are measured in a gravitational field, usually 1 g, in which the free convection phenomenon controls the combustion process; therefore, the last term in Eq. (9) is negligible. It is assumed that the functional relationship for the convective linear burning rate of a sample (β_s) can be expressed in a product form. Then, if conditions in which β_s was measured are known, it is possible to estimate a burning rate β for the same material for any other condition by ratioing the various functional terms such that

$$\frac{\beta}{\beta_s} = \left(\frac{l}{l_s}\right)^n \left(\frac{g}{g_s}\right)^n \frac{\theta}{\theta_s} \frac{f(P_{T_1}P_{O_2}}{f_s(P_{T_1}P_{O_2}} \quad (10)$$

Note that β includes the effects of convection, conduction, and radiation, whereas β^* is uniquely defined as the convective portion of the total linear burning rate.

If a particular geometry is assumed, the resistances and capacitances can be expressed in terms of the assumed physical properties and dimensions of the model. Based on the assumptions that 1) combustible materials are uniformly distributed, and 2) the rate of gaseous diffusion of O_2 to the flame front does not limit the combustion rate as long as oxygen exists, one can establish the equations for flame propagation.

From Eq. (8) and the definition of volume burning rates

$$\dot{q}_T = \phi[\gamma_c + \gamma_k + \gamma_r] = \phi\gamma_T \quad (11)$$

where γ_c is the convection portion of the volumetric burning rate. For a spherical surface, one would expect the radial burning rate (dr/dt) to be proportional to the linear burning rate of a flat surface. Two approaches could be used to determine the proportionality constant: 1) experimental correlation and 2) assumption of geometric equivalence. Because of the lack of experimental data, the second approach is used. Consider the two-dimensional model in Fig. 3. Assuming that the geometry is so maintained that dl/dt is equal for both burning faces, one can express

$$\alpha = \left.\frac{dA}{dt}\right|_l = 2l\frac{dl}{dt} = 2l\beta$$

Now assume that the burning area is spherical in topology of radius r such that

$$A_{\text{sphere}}\ (=4\pi r^2) = A_{\text{flat plate}}\ (= l^2)$$

Hence, by differentiation and by substitution of β for dl/dt

$$dr/dt = \beta/2(\pi)^{1/2} \quad (12)$$

For a spherical model

$$\beta = \beta_s^* \left(\frac{r}{r_s}\right)^n \left(\frac{g}{g_s}\right)^n \frac{\theta}{\theta_s} \frac{f(P_{T_1}P_{O_2})}{(f_sP_{T_1}P_{O_2})} \quad (13)$$

If Eq. (13) is substituted into Eq. (12) and integrated, r is obtained as a function of time t; by neglecting the implied relationships between $\theta_f(P_TP_{O_2})$, r, and t, the following expression for r is derived:

$$r = \left[\frac{1}{2}(1-n)\frac{\beta_s}{(\pi)^{1/2}r_s^n}\left(\frac{g}{g_s}\right)^n \frac{\theta}{\theta_s}\frac{f(P_T,P_{O2})}{f_s(P_{T_1}P_{O_2})}t + r_1^{1-n}\right]^{1/(1-n)} \quad (14)$$

Let us now derive each term in Eq. (14). The exponent n is derived from heat-transfer analogy. Because of the small dimensions of the sample strip for determining β, the process remains linear. The heat-transfer expression for free convection[4] for a flat plate is

$$Nu = C_1(GrPr)^{1/4} \quad (15)$$

while the expression for forced convection[4] for a flat plate is

$$Nu = C_2(Re)^{1/2}(Pr)^{1/3} \quad (16)$$

§ The vaporization or condensation term q_v was found to be negligible, and was dropped in the numerical solution of Eqs. (6) and (7).

When the oxygen-rich gas in the compartment flows into the combustion region, a gas velocity is generated which either rapidly propagates the flame or reduces the combustion process to a pure diffusion flame (as has been suggested for zero-g fires). A transition velocity may be defined as the value for which the heat-transfer rate due to forced convection equals the rate due to free convection. By Eqs. (15) and (16), a transition convection velocity can be defined, i.e., a velocity which, if exceeded, would make the combustion process velocity-sensitive;

$$v_t = C_3\mu(Gr)^{1/2}(Pr)^{-1/6}/\rho L_t$$

Since Pr is a function of the fluid properties only, $v_t \propto L_t^{1/2}g_t^{1/2}$, therefore $v/v_s = (L/L_s)^{1/2}(g/g_s)^{1/2}$ if $v > v_t$ and $v_s > v_t$. By analogy, a burning velocity ratio β/β_s can be expressed as

$$\beta/\beta_s = (l/l_s)^{1/2}(g/g_s)^{1/2}$$

Thus, the exponent n used in Eqs. (9, 10, 13, and 14) is $n = \frac{1}{2}$. Note that β_s values are experimental burning rates, and the fact that the flame front propagated along the length of the specimen implies that the transition burning velocity was exceeded.

It has been reported by McAlevy et al.,[5] that there is a power-law dependency of the linear burning rate on total system pressure (P_T) and oxygen mole fraction (Y_{O_2}):

$$\beta \propto Y_{O_2}{}^x P_T{}^y \tag{17}$$

where x = experimentally determined factor, primarily a function of diluent, >1; and y = experimentally determined factor, primarily a function of material, <1. It is recognized that correlation (Eq. 17) was based on the flammability data of two specific materials; however, the power-law dependency appears rational, and, therefore, one should not expect any change in the form of the expression but only in the experimentally derived factors. This correlation corrects for the diffusion phenomenon in the combustion process, and we assume that it can be used to define the pressure-dependent term in Eq. (9). By rearranging Eq. (17), we obtain

$$\beta/\beta_s = [(P_T/P_{T_s})^{x-y}(P_{O_2}/P_{O_{2s}})^y]^\psi \tag{18}$$

where the exponent ψ is introduced as a variable in order to utilize the McAlevy correlation in Eq. (13). This parameter should also account for any variation in the experimentally determined power factor resulting from material variation.

The θ in Eq. (13), which obviously has some effect on the linear burning rate, is the toplogical function. It relates the effect of geometric orientation of the specimen being burned on the specimen burning rate. However, because we have no data on this relationship, we assume that $\theta/\theta_s = 1$. If we substitute into Eq. (14)

$$\Lambda \equiv \frac{\beta_s}{4(\pi r_s)^{1/2}}\left(\frac{g}{g_s}\right)^{1/2}\frac{f(P_T,P_{O_2})}{f_s(P_T,P_{O_2})}$$

then, with $n = \frac{1}{2}$, we obtain

$$dr/dt = 2\Lambda[\Lambda t + r_i^{1/2}]$$

Because of the inherent differences in local material density and over-all average material density, a term ξ is introduced to account for this difference in the volumetric flame propagation rate: $\xi \equiv \phi'/\phi$. Further, when $g > 0$, $\gamma_c = f(\beta)$, and

$$\dot{q}_\beta = \dot{q}_{\beta_1} + \dot{q}_{\beta_2} \tag{19}$$

$$\dot{q}_\beta = \xi\phi\gamma_c = \xi\phi 4\pi r^2(dr/dt) \tag{20}$$

Substituting $r^2(dr/dt)$ into Eq. (20) yields

$$\dot{q}_\beta = \xi\phi(4\pi)2\Lambda[\Lambda t + r_i^{1/2}]^5 \tag{21}$$

Equation (11) can be rewritten in the following form:

$$\dot{q}_T = \dot{q}_\beta + \dot{q}_k + \dot{q}_r = \phi\gamma_T \tag{22}$$

If we substitute Eq. (21) into Eq. (22) and note that $\gamma_T = 4\pi r^2(dr/dt)$, we find, for a 1-$g$ field,

$$\frac{dr}{dt} = \frac{2\Lambda\xi[\Lambda t + r_i^{1/2}]^5}{r^2} + \frac{\dot{q}_k + \dot{q}_r}{4\pi r^2\phi} \tag{23}$$

For a 0-g field, the first term goes to zero.

Note that β as used in this analysis includes only the convective portion of the linear burning rate which in a 1-g field is the controlling term. However, in a 0-g field, the controlling terms are conduction and radiation. This definition of β was used in this analysis to simplify the propagation rate equation in a 0-g field.

Solution of the Basic Equations

By substituting Eqs. (3–5) into Eqs. (6) and (7), the following differential equations are obtained:

$$\frac{dT_g}{dt} + \frac{1}{C_g}\left(\frac{1}{R_k} + \frac{1}{R_c}\right)T_g - \frac{1}{C_g}\left(\frac{T_f}{R_k} - q_{\beta_1}\right) - \frac{T_m}{C_gR_c} = 0 \tag{24}$$

$$\frac{dT_m}{dt} + \frac{1}{C_m}\left(\frac{1}{R_c} + \frac{1}{R_r}\right)T_m - \frac{1}{C_m}\left(\frac{T_f}{R_r} + q_{\beta_2}\right) - \frac{T_g}{C_mR_c} = 0 \tag{25}$$

From the equation describing the chemical reaction assumed to occur during the combustion process, combined with the principle of the conservation of mass, one can determine the mass of any component of the gaseous phase from an equation of the form

$$W(t) = W(0) + A\int_0^t \frac{[4\pi r^2\phi(dr/dt)]}{\Delta h_c}\,dt \tag{26}$$

where A is a positive or negative conversion constant determined for each of the gaseous components of the atmosphere. For the combustion process described by Eq. (2), A has values of -2.29, $+1.57$, and $+1.29$ for O_2, CO_2, and H_2O (vapor), respectively.

By solving Eqs. (23) and (24–26), simultaneously, the desired solutions obtained are $T_g = T_g(t)$, $T_m = T_m(t)$, $r = r(t)$, and $W = W(t)$. Further, by utilizing the equation of state, it is possible to compute the atmospheric pressure history in the compartment $P_T = f(T_g,W) = f(t)$. A computer program incorporating a Runge-Kutta subroutine was used to solve the simultaneous differential equations numerically.

Comments on Mathematical Model

The model, as developed from the simple three-node approximation, may appear to be too crude to provide any useful information. More complex models (more nodes) were considered and eliminated because slight improvements in the lumped parameter approximation resulted in greatly increased mathematical complexity. The 3-node model takes into account all the major elements which would influence a fire, but it tends to give conservative results, because in an actual fire 1) the combustion process would be terminated before complete oxygen depletion, 2) the flame temperature would be reduced by the diffusion barrier of the combustion products,

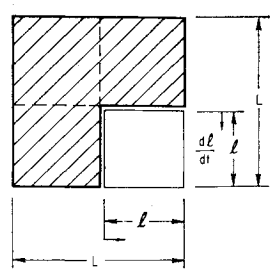

Fig. 3 Two-dimensional model.

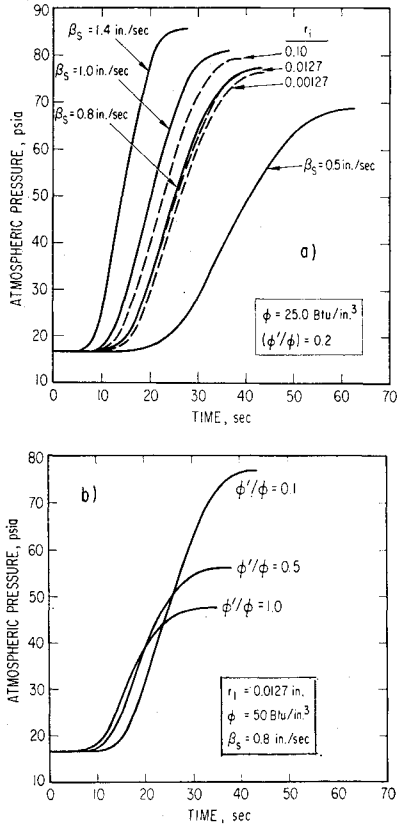

Fig. 4 Effects of a) linear burning rate β_s and initial ignition size r_i, b) volumetric heat of combustion ratio (ϑ°/ϕ), and c) total pressure and O_2 concentration correction on pressure history for a fire in a P_i = 16.5 psia, 100% O_2, 1-g field with r_0 = 15 in.

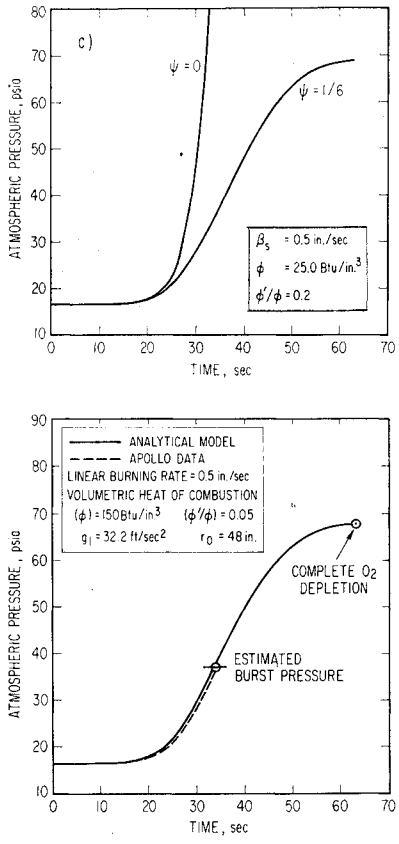

Fig. 5 Pressure history during a fire in a 16-psia, 100% O_2 atmosphere.

thereby slowing the process, and 3) energy would be lost from the system as the assumption of adiabatic exterior surfaces becomes marginal during the lengthening of the process time. The inclusion of any or all of these effects in the model would have a tendency to lower the predicted resultant pressure and decrease the predicted rate of combustion, thereby increasing the time to completion or extinguishment.

Discussion and Results

Figure 3a shows that for a 16.5-psia, pure-O_2 atmosphere, the time to reach 40 psia is increased less than 15 sec by changing from a linear burning rate of 0.8 in./sec to 0.5 in./sec. As a point of reference, the linear burning rate of Nylon Velcro in a 16 psia, 100% O_2 environment is 0.7 in./sec. The curves terminate at complete oxygen depletion.

By the dashed curves, Fig. 2a also shows the effect of r_i for the case β_s = 0.8 in./sec. As r_i decreases from 0.10 to 0.00127 in., the atmospheric pressure rise is delayed. The model showed that an asymptotic pressure history is reached for $r_i \leq$ 0.00127 in. However, it has been shown[5] that the quenching distance of a gas phase ignition is approximately 50μ (0.0127 in.) in a 1-g field, hence, an r_i of 0.0127 in. was used as a constant initial radius in the model for 1-g fires. It should be noted that an r_i of 1 in. was necessary in the analysis of 0-g fires to "sustain combustion"; this implies that the initiation of a fire in 0-g field is relatively difficult.

Because of the inherent difference in local material density and over-all average material density, the term ϕ'/ϕ was introduced to account for the differences in the volumetric heats of combustion. Figure 3b shows that as ϕ'/ϕ increases, the pressure reaches its peak value faster. This parameter gives an indication of the effect of relative packing densities, i.e., the fraction of the combustible material that would propagate the flame at β_s = 0.8 in./sec. In the model, the mass of the materials is used in two ways: 1) total mass of the system is used in the heat balance equation as a heat sink, and 2) the mass of the combustibles is used to partially characterize the energy content of the fuel at or near the combustion region in the flame propagation equation. It is the latter mass which is used in the definition of volumetric heat of combustion. Note that ϕ' is defined locally, i.e., ϕ' is defined only for the combustible materials in the vicinity of the flame front. The heat of combustion for spacecraft materials varies from a low of 2500 Btu/lb for materials such as Teflon to 14,000 Btu/lb for materials such as Nylon Velcro. The bulk densities of typical nonmetallic spacecraft material can vary from 0.0001 lb/in.^{3} to 0.05 lb/in.^{3} Figure 3b shows that the peak of the atmospheric pressure rise during a fire decreases with increasing values of volumetric heat of combustion ϕ: It should be noted that the linear burning rate is also dependent on the material and that varying ϕ' while fixing β_s as shown in Fig. 3b may not be physically possible; however, the figure does show a semiquantitative dependence of atmosphere pressure history on ϕ'.

Figure 3c shows the effect of ψ. Because of the way that β is used in this analysis, ψ can range from 0 to $\frac{1}{6}$. A value of $\frac{1}{6}$ would be comparable to a McAlevy correction based on volumetric burning rate. It is interesting to note that the ψ correction strongly affects the termination or end point of the fire. The S-shape curve associated with $\psi = \frac{1}{6}$ can be explained as follows: Initially, the surface area of the flame front is small, and most of the energy is consumed in heating the adjacent structure. As the size of the flame front increases, the convective term predominates, thereby raising the temperature and pressure of the gas. Finally, as P_{O_2} decreases, and P_T increases, the convective linear burning rate contribution is reduced due to oxygen diffusion limitations (as expressed by the McAlevy correlation), such that the rate of combustion is progressively reduced until all O_2 is consumed. A ψ equal to zero implies that the O_2 and fuel supplied to the flame front are premixed for the entire combustion process, such that the diffusion rates of gases to and from the flame front do not affect the burning rate. Specifically, the combustion rate is not reduced by either the decreasing P_{O_2} or the increasing P_T.

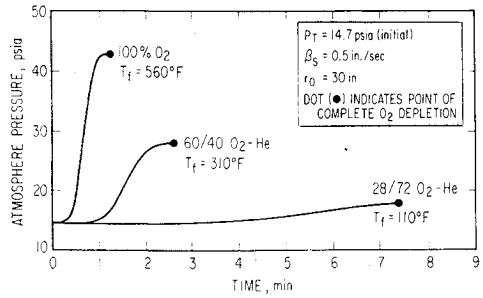

Fig. 6 Pressure history of a closed compartment atmosphere during a fire on the ground (1 *g*).

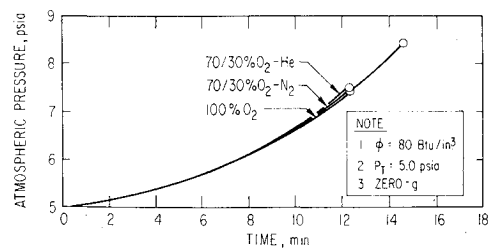

Fig. 7 Pressure history of a closed compartment atmosphere during a fire on-orbit.

Apollo Correlation

A comparison of the pressure history of the Apollo 204 fire, as reported by NASA,[6] and the pressure history of an Apollo type atmosphere (16 psia, 100% O_2) is shown in Fig. 4. By the proper selection of β^*, ϕ, and ϕ'/ϕ, a good correlation was achieved. The β^* value of 0.5 in./sec. (averaged for the spacecraft) seems reasonable for the Apollo because of the extensive use of Nylon Velcro in the command module at the time of the fire. In the Apollo fire, the typical S-shape pressure curve was probably not experienced, because the pressure vessel burst during the increasing convective portion of the combustion process, and the effect of the decrease in P_{O_2}, and the increase in P_T was negligible at the point of rupture.

The use of a fixed-volume compartment in this analysis predicts higher pressures than would be realized in an actual spacecraft fire in which a relief valve would allow atmospheric gas outflow once a preset cabin pressure level were reached. For slowly propagating fires (i.e., where flame propagates in minutes instead of seconds), the assumption of a fixed-volume compartment is conservative since the relief valve could be sized so that the gas outflow would be more than sufficient to offset the atmospheric pressure increase due to combustion.

Typical Closed Compartment Fire

Three typical ground-test and launch pad atmospheres were examined, viz.: 1) pure O_2, 2) 60% O_2, 40% He, and 3) a 28% O_2, 72% He, all at 14.7 psia. Figures 5–7 show the pressure histories and final atmospheric temperatures for these cases. With 100% O_2 the pressure would increase by ~28 psi in 1.2 min. With 60% O_2, the pressure rise is ~13 psi in 2.5 min; with 28% O_2, only 3 psi in 7.5 min. The times quoted are the times to extinguishment by complete oxygen depletion. The β_s and ϕ values used were identical to those established by the Apollo correlation.

Two typical spacecraft atmospheric modes on-orbit, both with an initial P_T of 5 psia, are examined in Fig. 4. The 100% O_2 atmosphere burns longer and reaches higher pressure and temperature levels at O_2 depletion primarily because of the greater O_2 mass associated with it. The maximum predicted pressure and temperature rise for the 100% O_2 mode are 3.5 psi and 70°F, respectively. In a 70% O_2-30% diluent atmosphere, there is no noticeable difference in the diluent effect of He vs N_2. However, there is an advantage favoring He, namely, that ignition in an He-O_2 atmosphere requires more energy because of its relatively high thermal conductivity.

Conclusions and Recommendations

A simple, spherical analytical model of a fire in a closed compartment indicates that:

1) With an initial on-orbit (0-*g*) cabin atmosphere of 100% oxygen at 5 psia the atmospheric pressure increase will be less than 4 psia and the temperature will be less than 150°F if appreciable oxygen is not introduced during the fire.

2) The use of a two-gas atmosphere is a highly effective approach for reducing a cabin fire hazard in a gravitational field.

3) The most critical cabin fire potential occurs in a gravitational field.

Based on the results of this study, it is recommended that further tests and studies be conducted to verify the utility of the oxygen depletion concept for cabin fire extinguishment, and that the minimum practicable atmospheric O_2 partial pressure be utilized in any ground operation (e.g., testing, storage, pad).

References

[1] Von Elbe, G. et al., "Quantitative Guidance for Material Control to Minimize Fire Hazards in Spacecrafts," Preliminary Draft of Task I Report, NASA Contract NAS 9-7057, Sept. 1967, Atlantic Research Corp., Alexandria, Va.

[2] Bonura, M. S. et al., "Engineering Criteria for Spacecraft Cabin Atmosphere Selection," DACO Rept. DAC-59169, Contract NASA 1371, Nov. 1966, Douglas Aircraft Co., Santa Monica, Calif.

[3] McAdams, W. H., *Heat Transmission*, 3rd ed., McGraw-Hill, New York, 1954.

[4] Kimzey, J. H., "Flammability in a Zero Gravity Environment," TR-R246, Oct. 1966, NASA.

[5] McAlevy, R. F. et al., "Flame Spreading at Elevated Pressures Over the Surface of Igniting Solid Propellants and Propellant Ingredients in Oxygen/Inert Environments," Annual Report ME-RT 67011, Oct. 1967, Stevens Institute of Technology, Hoboken, N. J.,

[6] "Report of Apollo 204 Review Board," NASA Final Rept., April 1967, F. L. Thompson, Chairman.